Check for updates

AGU ADVANCING EARTH AND SPACE SCIENCE

JGR Atmospheres

RESEARCH ARTICLE
10.1029/2019JD031172

Special Section:
A NEW ERA OF LIGHTNING OBSERVATIONS FROM SPACE

Comparisons of Lightning Rates and Properties From the U.S. National Lightning Detection Network (NLDN) and GLD360 With GOES-16 Geostationary Lightning Mapper and Advanced Baseline Imager Data

Martin J. Murphy[1] **and Ryan K. Said**[1]

[1]Vaisala Inc., Louisville, CO, USA

Key Points:
- Geostationary Lightning Mapper detection efficiency decreases within 2,000 km of edge of field of view over the western United States
- Flash rates often do not correlate well between Geostationary Lightning Mapper and National Lightning Detection Network
- Low Geostationary Lightning Mapper detection efficiency appears to correlate with a combination of various factors

Supporting Information:
- Supporting Information S1

Correspondence to:
M. J. Murphy,
martin.murphy@vaisala.com

Citation:
Murphy, M. J., & Said, R. K. (2020). Comparisons of lightning rates and properties from the U.S. National Lightning Detection Network (NLDN) and GLD360 with GOES-16 Geostationary Lightning Mapper and Advanced Baseline Imager data. *Journal of Geophysical Research: Atmospheres*, *125*, e2019JD031172. https://doi.org/10.1029/2019JD031172

Received 14 JUN 2019
Accepted 8 FEB 2020
Accepted article online 14 FEB 2020

©2020. American Geophysical Union. All Rights Reserved.

Abstract Flash-level comparisons between the Geostationary Lightning Mapper (GLM; primarily from GOES-16), the U.S. National Lightning Detection Network (NLDN), and the Global Lightning Dataset GLD360 have been done at quasi-climatological scale and in smaller samples of both severe and nonsevere thunderstorms. A small sample of data from GOES-17 has also been analyzed. These comparisons show that the total lightning detection efficiencies of the GLM instruments drop off within about 2,000 km of the edges of their fields of view, particularly over terrestrial areas. In severe storms, low detection efficiency by GLM is clearly associated with very high midaltitude reflectivity, consistent with the idea that large multiple scattering path lengths, together with absorption of the near-infrared signals by water (in all of its phases), depresses the GLM detection efficiency. This effect appears to be coupled with additional factors, including time of day, flash energetics, and the incident angle at the GLM sensor. The "lightning jump," the sought-after signature of severe storms in lightning observations, tends to be poorly correlated between NLDN and GLM unless the storms are fairly isolated, not close to the edge of the GLM field of view, and have moderate midaltitude reflectivity.

1. Introduction

The Geostationary Lightning Mappers (GLM) on the GOES-16 and -17 satellites (Goodman et al., 2013), as well as an analogous instrument called the Geostationary Lightning Imager on China's Fengyun-4A satellite (Yang et al., 2017), have as primary mission objectives to provide total lightning detection and spatial mapping over large continent- to planetary-scale areas including significant swaths of ocean. Such large areas are also covered by ground-based lightning locating systems (LLSs) such as the Global Lightning Dataset (GLD360) and U.S. National Lightning Detection Network (NLDN). However, despite substantial advances in the cloud lightning detection capabilities of ground-based LLSs over the recent 5 years, such systems are not (arguably; see, e.g., Murphy & Said, 2018) considered "total lightning" detection systems, nor do they provide complete spatial mapping of flashes. The GLMs and analogous instruments achieve total lightning mapping by observing near-infrared emissions at 777.4 nm wavelength from lightning after they are scattered through the clouds and emerge from cloud tops. These emissions are then detected on a charge-coupled device (CCD) array whose pixel size at nadir corresponds roughly to the size of the smallest thunderstorm clouds, about 8 km * 8 km.

One of the stated objectives of satellite lightning mappers is to provide uniformly high total lightning detection efficiency (DE) of 70–90% over a large field of view spanning roughly 104° of latitude (from −52 to +52 latitude) and an equivalent amount in longitude (Goodman et al., 2013).

Another of the primary objectives of satellite lightning mappers is to provide the continuous temporal coverage of total lightning observations over wide areas that is necessary in order to capture the development of severe thunderstorms. As defined in the United States, "severe" thunderstorms are those that produce a tornado, hailstones with a diameter of at least 2.54 cm, or wind of at least 25.8 m/s (https://www.spc.noaa.gov/faq/#4.2). The literature review provided by Schultz et al. (2011) shows the extensive history of analyses of severe thunderstorms using only CG lightning information and indicates that total lightning observations are necessary to capture the complete relationship between the strength of thunderstorm updrafts, which ultimately propel the severe weather "engine," and the readily observable electrical manifestation of these in the form of lightning. Specifically, numerous studies have shown that there is a

relationship between rapid increases in total flash rate, known as "lightning jumps," and the likelihood of the subsequent production of severe weather (see Chronis, Carey, et al., 2015; Schultz et al., 2011; Schultz et al., 2015; Schultz et al., 2017; Williams et al., 1999, and references therein). According to a number of these authors, one of the primary goals of satellite lightning mappers is severe weather warning enhancement via the lightning jump.

Although the exact timing and number of lightning jumps depend on the thresholds applied to the time derivative of flash rate (Chronis, Carey, et al., 2015), the lightning flashes associated with lightning jumps in general differ from lower flash rate situations. Specifically, an inverse relationship between the size of lightning flashes and the rate of flashes has been observed (Bruning & MacGorman, 2013). Higher rates of smaller flashes tend to occur in the presence of more vigorous convective updrafts, which are also more turbulent. Such updrafts lead to a more finely textured organization of charge within the thunderstorm, which in turn appears to lead to lightning flashes with smaller spatial scales. Possibly, the reorganization of charge by the (more frequent) lightning flashes themselves may also contribute to this textured charge structure. This could potentially reinforce the tendency toward smaller flashes in high flash-rate storms. All of these behaviors present a challenge to the use of satellite lightning mappers to detect lightning jumps, as Zhang and Cummins (2019) have noted that the DE of the GLM on GOES-16 is significantly lower in the case of small, short-duration flashes. Indeed, Curtis et al. (2018) found, in the first comparison of lightning jump observations between the GOES-16 GLM and Lightning Mapping Arrays (LMAs; Thomas et al., 2004), that significant discrepancies exist between the total flash rates and lightning jumps observed by the LMAs and the GLM.

In addition to the inverse relationship between flash size and flash rate, additional confounding factors have been shown in presentations at the 99th American Meteorological Society annual meeting by Hilburn et al. (2019; see https://ams.confex.com/ams/2019Annual/videogateway.cgi/id/50561?recordingid=50561) and Thomas et al. (2019; see https://ams.confex.com/ams/2019Annual/videogateway.cgi/id/50728?recordingid=50728). Specifically, storms over the high plains of eastern Colorado tend to produce a large proportion of low-altitude cloud flashes given the tendency of these storms toward anomalous electrical charge structure (Bruning et al., 2014), whereas storms in the southeastern United States typically produce more cloud flashes at higher altitudes. That difference alone leads to a significant difference in the amount of ice between the tops of the lightning flashes and the tops of the clouds. That, in turn, appears to result in a significant difference in the amount of multiple scattering and absorption of the near-IR signals to be detected by the GLM and, thus, an overall reduction in flash DE by the GLM.

Factors associated with the amount of ice are now observable from satellite over wide areas by virtue of the introduction of the Advanced Baseline Imager (ABI) instruments (Schmit et al., 2017) on the GOES-16 and -17 satellites. The ABIs have 16 channels extending from the visible into the thermal infrared, instead of the five channels available on the previous operational GOES cloud imagers. The higher spectral resolution of the ABIs facilitates the calculation of derived cloud products, including cloud top altitude, rain rate/quantitative precipitation estimation (hereafter, "RRQPE"), and cloud optical depth, which were not available from previous-generation imagers. Perhaps, in the absence of detailed observations of the ice water path between lightning flashes and cloud tops, the combination of ABI with GLM observations might lead to insights about GLM flash rates, DE, and lightning jumps, which, in turn, might lead to refinements in how GLM observations might be used in severe weather monitoring.

Yet another confounding factor resides in how a lightning flash is defined. To date, almost all studies of lightning jumps (e.g., Chronis, Carey, et al., 2015; Curtis et al., 2018; Gatlin & Goodman, 2010; Schultz et al., 2009, 2011; Schultz et al., 2015; Schultz et al., 2017) have been conducted using LMAs, with a few other studies based on other VHF lightning mapping systems with high spatial resolution (e.g., Farnell et al., 2017). However, the difference in flash clustering algorithms between LMAs and other VHF mapping systems might introduce differences in lightning jumps, an issue worthy of future work. Even worse, given just a single source of high-resolution VHF observations, flash rates higher than about 60 min^{-1} can vary significantly just by variations in the configuration of the flash clustering algorithm (Murphy, 2006) and thus are inherently difficult to quantify. The comparison between flashes as defined by different types of LLS, such as GLM and LMAs, makes it even more likely that there could be discrepancies in flash rates and lightning jumps.

21698996, 2020, 5, Downloaded from https://agupubs.onlinelibrary.wiley.com/doi/10.1029/2019JD031172 by Capes, Wiley Online Library on [01/10/2025]. See the Terms and Conditions (https://onlinelibrary.wiley.com/terms-and-conditions) on Wiley Online Library for rules of use; OA articles are governed by the applicable Creative Commons License

Given all of the above considerations, our objectives in this paper are the following. First, we seek to provide an analysis of GLM DE over a broad scale by showing flash-level comparisons. We show a 10-month period with respect to the NLDN over the continental United States and a nearly 14-month period with respect to the GLD360 over the entire GLM field of view. Then, we examine a number of small, isolated storms with low flash rates over the western United States. These storms are selected specifically to avoid the problems of high flash rates and complex, multicellular storms. This allows us to examine the relative DE without the confounding factors of flash clustering and flash definitions. Finally, with respect to severe storms, we seek to build upon the results of Curtis et al. (2018) by examining a sample of severe storms using GLM and ABI data, but this time using NLDN rather than LMA as the source of ground-based total lightning observations against which the GLM data are compared. Although the lightning jumps are of interest in the severe storm cases, we also examine the GLM and NLDN flash rate time series throughout the storm life cycles. In this analysis of severe storms, we also explicitly control for factors that might reasonably be expected to relate to the GLM's DE, such as storm morphology. This is an important factor given that Zhang and Cummins (2019) have shown that small, short-duration flashes are not as well detected by GLM as larger and longer flashes.

2. Data and Methods

Both severe and isolated nonsevere thunderstorm cases analyzed in this paper are from the summer of 2018. The nonsevere thunderstorms are all isolated, air mass thunderstorms over the intermountain western United States during late May to mid-June of 2018. The selected severe storm cases are partitioned into two groups by storm morphology, with one group composed of linear systems that later evolved into clusters or MCSs and the other group composed of supercells. Specifically, the selected severe storms are as follows:

1. 2018-06-19 00:00–03:00 UTC over northern Colorado (linear/clusters): A line of storms formed over the Boulder area after initially developing as isolated cells over the mountains. Large hail occurred in many areas to the east of Boulder between 01:00 and 03:00 UTC.
2. 2018-07-19 20:00–23:00 UTC over Iowa (supercells): A number of reasonably isolated supercells that produced EF0-EF3 tornadoes were observed on this day (NCEI, 2018).
3. 2018-07-29 20:00 UTC to 2018-07-30 03:00 UTC over Wyoming and Colorado (supercells): These were also supercells in most cases, although they evolved toward a linearly organized storm cluster later. Hail reports were predominant, with a few tornadoes also reported.
4. 2018-08-17 19:00–23:00 UTC over Virginia, Maryland, Pennsylvania, and New York (linear/clusters): This case consisted of a mix of fairly isolated cells and some linearly organized storms. Damaging wind reports were the exclusive severe weather reports from this case.
5. 2018-08-27 22:00 UTC to 2018-08-28 02:00 UTC over Minnesota and Wisconsin (linear/clusters): Toward the southern end of this system, the storms were linearly organized. Farther north, a couple of MCSs developed. Most of the severe weather reports were of damaging wind, although a couple of tornado reports also came from southeastern Minnesota.

2.1. Lightning observations

During the selected severe and nonsevere storm cases, all from 2018, the GLM data from the GOES-16 satellite (centered at −75° longitude) were made available in netCDF format, with each file covering 20 s. GLM provides three levels of information: (1) "events," which are individual pixel illuminations with the GLM's native time resolution of 2 ms; (2) "groups," which are collections of adjacent events in the same 2-ms time window; and (3) "flashes," which are built from groups that overlap or are within 15 km in space and that are separated by no more than 330 ms in time (Goodman et al., 2013). In this work, "events" are ignored, but "flashes" are utilized in all flash rate analyses, and "groups" are shown in maps of individual storm cases. Because time-of-flight corrections were not made operational until autumn 2018, we introduced custom time corrections based on the position of the group or flash and the (fixed) satellite altitude and longitude for GLM data before the update. In early 2019, data from the GLM on GOES-17 (centered at −137° longitude) became available. A sample of these data was also used to elucidate DE issues, as described in section 3. However, because almost all GLM data in this paper are from GOES-16, unless otherwise indicated, we use "GLM" to refer to the GOES-16 GLM.

Ground-based LLS observations are taken from the NLDN and the GLD360. Recent performance validation by Zhu et al. (2016) shows a cloud flash detection efficiency of 73% and CG stroke detection efficiency of

21698996, 2020, 5, Downloaded from https://agupubs.onlinelibrary.wiley.com/doi/10.1029/2019JD031172 by Capes, Wiley Online Library on [01/10/2025]. See the Terms and Conditions (https://onlinelibrary.wiley.com/terms-and-conditions) on Wiley Online Library for rules of use; OA articles are governed by the applicable Creative Commons License

Table 1
Sensitivity of Number of Matched Flashes Between GLM and NLDN as a Function of Changes to the Maximum Distance and Maximum Time Window Gap Limits in the Matching Process

Maximum distance (km)	Maximum time window gap (ms)	# NLDN-GLM matched flashes	% Change relative to top row
20	200	1,584,541	—
10	200	1,281,347	−19.1
50	200	1,819,557	+14.8
20	100	1,521,976	−3.9
50	100	1,728,351	+9.1

92% in north-central Florida. Using a set of 11 storm cases near the Oklahoma and Colorado LMAs, Murphy and Nag (2015) found that the NLDN has total lightning flash detection efficiencies of 57.8% (Colorado) and 63.3% (Oklahoma). The NLDN observations in this paper are first reprocessed through an updated suite of central processing algorithms that became the operational NLDN central processing suite on 2018-11-07. Much more detail about the updated NLDN algorithms can be found in a presentation at the 99th American Meteorological Society annual meeting (Murphy, 2019; see https://ams.confex.com/ams/2019Annual/videogateway.cgi/id/50728?recordingid=50682). A paper based on that presentation is in progress.

Rudlosky et al. (2017) compared GLD360 (processed with the currently operational geolocation algorithm) to TRMM-LIS and found a total lightning flash detection efficiency of 44% over the Western Hemisphere with 3 years of data.

"Flashes" in both NLDN and GLD360 data are generated from the clustering algorithm described in Murphy and Nag (2015). All flashes from NLDN and GLD360 are used, whether or not they produced any cloud-to-ground (CG) strokes; thus, the comparisons presented here are total lightning comparisons.

2.2. Overall NLDN/GLD360—GLM Comparisons

The overall comparisons between NLDN/GLD360 and GLM in this study are flash-level comparisons. Flashes are considered "matched" if the flash positions are within 20 km of each other; 20 km corresponds to approximately 2 pixel widths on the GLM over the United States. The flash position in the case of GLM is the centroid position reported in the netCDF files. In the NLDN and GLD360, the flash position is the position of the first event (either IC pulse or CG stroke) in the flash. Flashes are considered "matched" in time if the flash time windows between the start and end times have a gap less than 200 ms. Flash start and end times are determined using all "groups" in GLM data and all events (both CG strokes and IC pulses) in NLDN and GLD360 flashes.

To examine the sensitivity of the comparisons to the matching criteria, we replayed the GLM and NLDN data from the four severe storm days that are discussed in detail in sections 3.4 and 3.5 below. The NLDN detected a total of 2,707,129 flashes on those 4 days, widely distributed over most of the continental United States. Table 1 summarizes the number of NLDN-GLM flash matches that we obtain when we vary the maximum distance between flash positions and maximum flash time window gap. The first row, 20 km and 200 ms, are the values mentioned above. When these limits are changed by factors of 2–2.5, the corresponding variation in number of matched flashes remains within ±20%.

The method of assessing the total lightning detection efficiencies of the NLDN/GLD360 and GLM is a two-way version of the three-way Bayesian approach presented by Bitzer and Burchfield (2016). Specifically, referring to GLM as "G" and NLDN or GLD360 as "N" in the following, the probability of detection by either system can be expressed as

$$P(N \cup G) = P(N) + P(G) - P(N \cap G). \tag{1}$$

Similarly, in this notation, Bayes theorem and the multiplicative law can be expressed as follows:

$$P(N|G) = P(G|N)\frac{P(N)}{P(G)}, \tag{2}$$

$$P(N|G) = \frac{P(N \cap G)}{P(G)}. \tag{3}$$

Finally, the maximum possible value, 1.0, of the probability in (1), $P(N \cup G)$, is translated into the upper bounds on the detection efficiencies of the GLM and NLDN, respectively, by combining the expressions (2) and (3), yielding (4) and (5):

21698996, 2020, 5, Downloaded from https://agupubs.onlinelibrary.wiley.com/doi/10.1029/2019JD031172 by Capes, Wiley Online Library on [01/10/2025]. See the Terms and Conditions (https://onlinelibrary.wiley.com/terms-and-conditions) on Wiley Online Library for rules of use; OA articles are governed by the applicable Creative Commons License

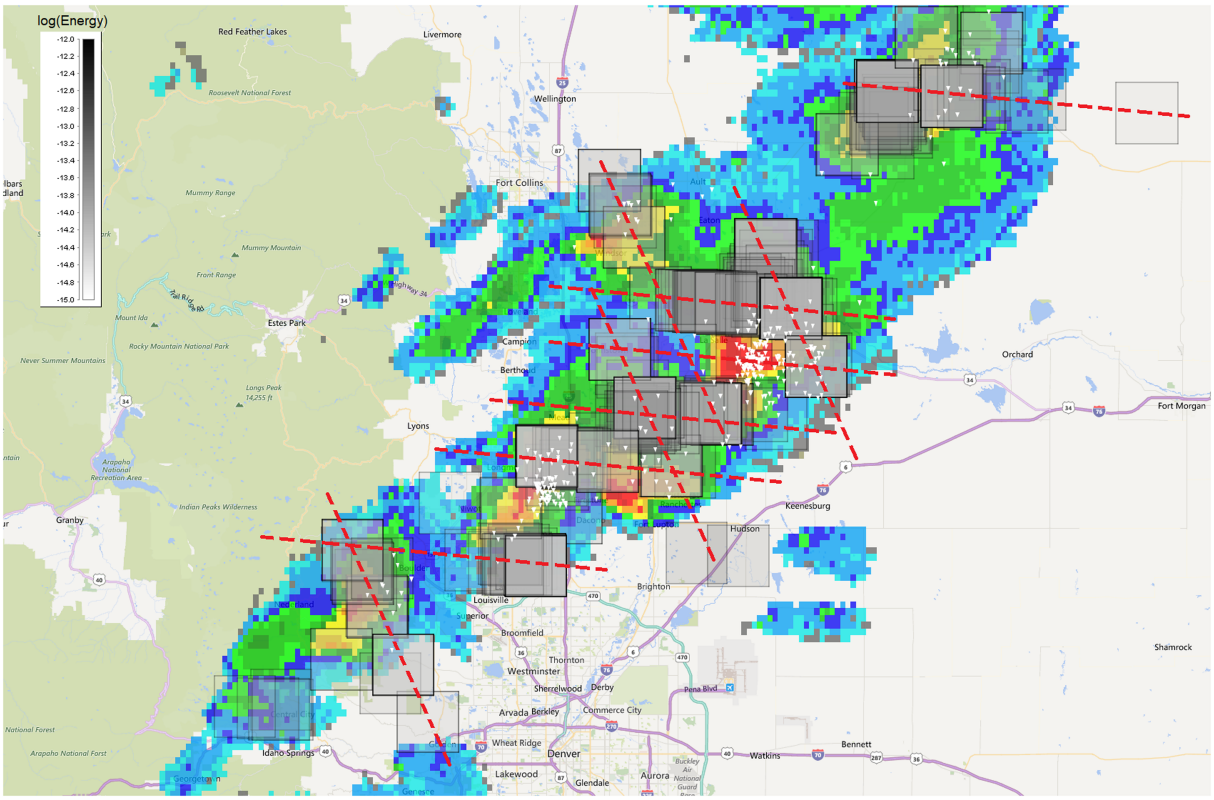

Figure 1. Radar (colors), GLM groups (10 × 10 km boxes, gray scale) and NLDN (small white dots) at 01:00 UTC on 2018-06-19 over northern Colorado. Notable observations are the alignment of most GLM group positions on a grid (red, dashed) and the relative lack of GLM observations directly over the storm cores that have the highest reflectivity.

$$P(G) \leq \frac{P(G)}{P(G \cup N)} = \left[1 - P(N|G) + \frac{P(N|G)}{P(G|N)}\right]^{-1}, \tag{4}$$

$$P(N) \leq \frac{P(N)}{P(G \cup N)} = \left[1 - P(G|N) + \frac{P(G|N)}{P(N|G)}\right]^{-1}. \tag{5}$$

The two conditional probabilities, $P(N|G)$ and $P(G|N)$, are readily observable from the process of matching flashes between the two data sets, as described above.

2.3. Thunderstorm Tracking in Individual Storm Cases

The means of tracking individual thunderstorms is described in Murphy (2017), and a detailed description is provided in the supporting information. In principle, the storm tracking algorithm should be equally applicable to NLDN and GLM data. However, in practice, it is found that the GLM data are simply too coarse in spatial resolution and, additionally, the GLM appears to have too low a DE in storm cores to allow the tracking method to work properly on GLM data alone. Figure 1 shows a comparison between radar, NLDN (small white dots) and GLM groups (10 × 10 km boxes, in shades of gray proportional to the logarithm of group energy) in a 2-min period of one of the severe storm cases selected in this work. Boxes of 10 × 10 km size are used to represent the GLM groups in this figure because that corresponds roughly to the size of a single GLM pixel when mapped to the location in question. Because so many GLM groups consist of just 1–2 optical "events," GLM group positions tend to align along a grid that reflects the CCD pixel array geometric mapping to this location. In Figure 1, this grid is highlighted with dashed, red lines. One other point from Figure 1 is to note that the storm cores with the highest reflectivities have little or no GLM groups directly over them, whereas plentiful NLDN events are clustered inside the storm cores. This could either be an issue of more light escaping the sides of the clouds than their tops, in which case the GLM data may be offset in

21698996, 2020, 5, Downloaded from https://agupubs.onlinelibrary.wiley.com/doi/10.1029/2019JD031172 by Capes, Wiley Online Library on [01/10/2025]. See the Terms and Conditions (https://onlinelibrary.wiley.com/terms-and-conditions) on Wiley Online Library for rules of use; OA articles are governed by the applicable Creative Commons License

position with respect to the storm cores, or it may be an issue of reduced DE of the GLM when the clouds are very optically thick. As discussed in section 3, the latter appears likely.

The alignment of GLM groups, shown in Figure 1, coupled with their spatial resolution, creates erratic storm tracks that are dramatically different from those provided by the NLDN, when the GLM flash data are applied to the same storm tracking algorithm. This discrepancy prevents direct storm track comparisons, and we avoid this problem by forming storm tracks exclusively from the NLDN data. Then, GLM flashes whose first group positions are within 25 km of the NLDN-based storm tracks are assigned to those storm tracks. The choice of 25 km should theoretically accommodate the possibility that lightning is detected from the sides rather than the tops of optically thick clouds. This choice could also result in the assignment of the same GLM flash to more than one storm track in cases of lines of storms or MCSs, where storm cell centroids can easily be closer together than 25 km. Our experience is that this misassignment can be a problem, but not in all cases of linear or clustered storm systems. Sometimes, GLM and NLDN flash rates agree well in linear or clustered storms. On that basis, we anticipate that the use of a 25-km maximum assignment distance probably produces only minimal bias in the flash rate and lightning jump comparisons between GLM and NLDN.

2.4. Lightning Jumps

Lightning jumps are calculated using the 2σ method of Schultz et al. (2011). The same method is applied to both NLDN and GLM data in this work. Although Murphy (2017) described the filtering of lightning jumps from NLDN data based on polarity and lightning type information, that approach is not used in this study because it obviously cannot be applied to GLM data. Thus, all lightning jumps in this work are "unfiltered" in the terms used by Murphy (2017).

2.5. Radar and ABI Data

Cloud properties are critical to understanding the DE of the GLM, and therefore, we use both ABI and radar data to investigate those properties. The ABI provides estimates of cloud top altitude, day and night cloud optical depth, and rain rate/quantitative precipitation estimate (hereafter RRQPE) products. However, the ABI day and night optical depth algorithms produce drastically different results. Thus, we instead examine the brightness temperature (BT) from Channel 7 in our severe storm cases because this channel is available both day and night and has reasonable temporal continuity across the terminator. As discussed in section 3.6, however, we find that the cloud top altitude and Channel 7 BT values vary little and correlate poorly with flash rates. Therefore, we resort to radar reflectivity, even though reflectivity is an imperfect proxy of cloud properties. Radar data are examined via the NOAA Weather and Climate Toolkit (https://www.ncdc.noaa.gov/wct/) in order to examine level-II NEXRAD data. Radar-relative AGL altitudes are converted to MSL altitudes and ultimately used to make vertical profiles of reflectivity in the storms of interest. These are then compared with ABI derived cloud attributes.

3. Results

3.1. Analysis of GLM DE—Large Scale

GLM flash DE relative to NLDN, as well as NLDN flash DE relative to GLM, is analyzed over a period of over 10 months from 2018-02-13 to 2019-01-01. Figure 2a presents the conditional probability $P(G|N)$ from equations (2)–(5) (i.e., the NLDN-relative DE of the GLM) using data from GLM on the GOES-16 satellite. As mentioned above, this probability calculation includes all flashes from the NLDN. Figure 2b presents the complementary value, $P(N|G)$. The resolution of both maps is 1° in both latitude and longitude. We note that $P(G|N)$ contains a broad swath of low relative detection efficiencies over the western United States and extending toward the north-central United States. The values of $P(G|N)$ range from 0.2 to 0.4 over most of that region. The values of $P(N|G)$ are higher over this area, although there patches in the central Rocky Mountains where the values are around 0.4. Section 3.2 goes into a detailed analysis of a set of small, isolated, low-flash-rate storms over the western United States in order to shed more light on the performance of both systems over this region.

The upper bounds on the total lightning DEs of the individual systems, the NLDN and GLM individually, derived from equations (4) and (5), are presented in Figures 3a and 3b. Figure 3a shows that the inferred upper bound on the total lightning DE of the NLDN ranges from about 0.6 to 0.9 over the continental

21698996, 2020, 5, Downloaded from https://agupubs.onlinelibrary.wiley.com/doi/10.1029/2019JD031172 by Capes, Wiley Online Library on [01/10/2025]. See the Terms and Conditions (https://onlinelibrary.wiley.com/terms-and-conditions) on Wiley Online Library for rules of use; OA articles are governed by the applicable Creative Commons License

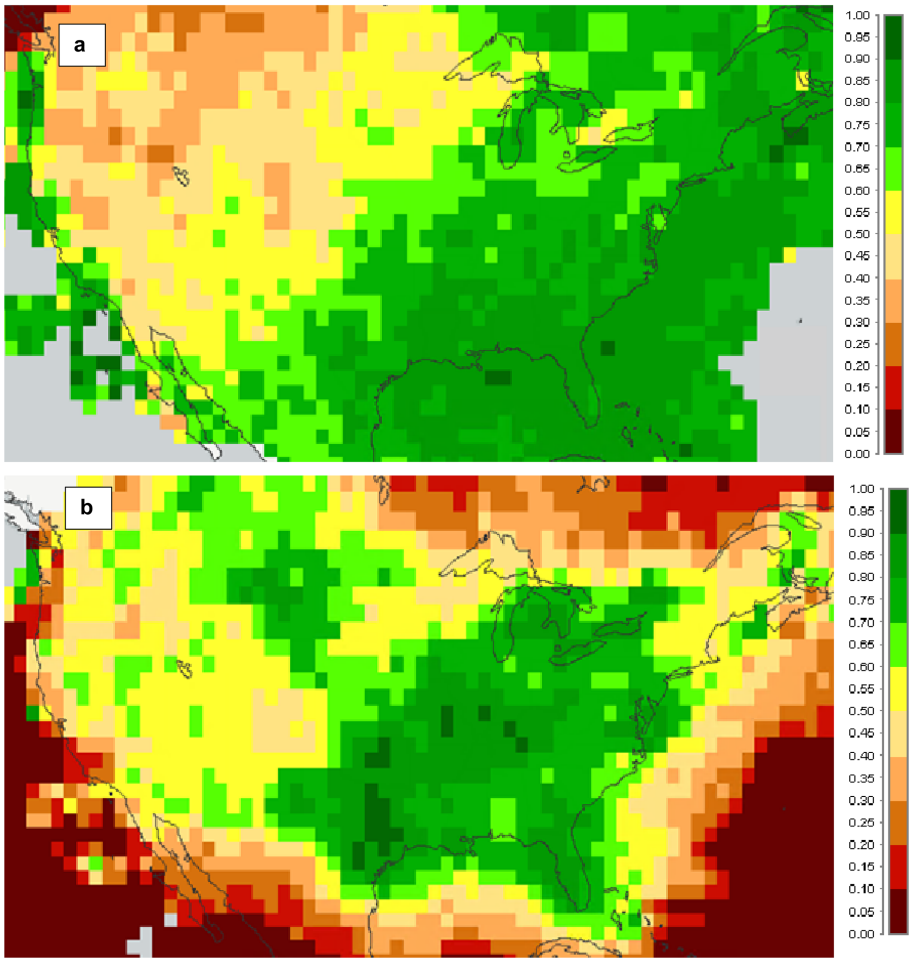

Figure 2. (a) NLDN-relative total lightning DE of the GLM, $P(G|N)$, over the period 2018-02-13 through 2019-01-01. Color scale from 0.0 to 1.0 is shown at right. (b) GLM-relative total lightning DE of the NLDN, $P(N|G)$, 2018-02-13 through 2019-01-01. Color scale from 0.0 to 1.0 is shown at right.

United States and drops off as expected off the coasts and over Mexico. The upper bound on the GLM DE is mostly between 0.7 and 0.8, as expected, over the eastern 1/3 of the continental United States but drops to the range of 0.3 to 0.5 over most of the western 2/3 of the United States. As expected, with respect to the NLDN, the upper bound on the GLM DE is substantially higher off the coasts and over Mexico, where the NLDN DE is expected to drop off.

Figure 4 shows the conditional flash DE of the GLMs on both GOES-16 and GOES-17 using GLD360 as a reference. As in Figure 2b, the DE falls off in the western United States. However, the DE falloff in the other three corners of the field of view appears to be much less dramatic. Using data from NLDN or GLD360, we are unable to test directly the dependence of DE on flash size and optical depth. However, we can estimate the dependence on peak current (which we take here to be a crude proxy for the optical brightness of the emission) and local time. Figures 4a and 4b show the conditional probability for GLD360 flashes with a peak current magnitude less than 10 kA (4a) and greater than 10 kA (4b). Similarly, Figures 4c and 4d show the DE over 08:00–16:00 local solar time (LST) and 18:00–06:00 LST, respectively, roughly capturing daytime and nighttime conditions. Finally, Figures 4e and 4f show the relative flash DE with no peak current or time-of-day filter of the GOES-16 and GOES-17 GLMs.

Figure 4 shows that the DE improves a little with higher peak current magnitudes compared to lower peak current magnitudes, and at night versus day (Boccippio et al., 2002). A complex mixture of factors appears to be in play in the overall pattern.

21698996, 2020, 5, Downloaded from https://agupubs.onlinelibrary.wiley.com/doi/10.1029/2019JD031172 by Capes, Wiley Online Library on [01/10/2025]. See the Terms and Conditions (https://onlinelibrary.wiley.com/terms-and-conditions) on Wiley Online Library for rules of use; OA articles are governed by the applicable Creative Commons License

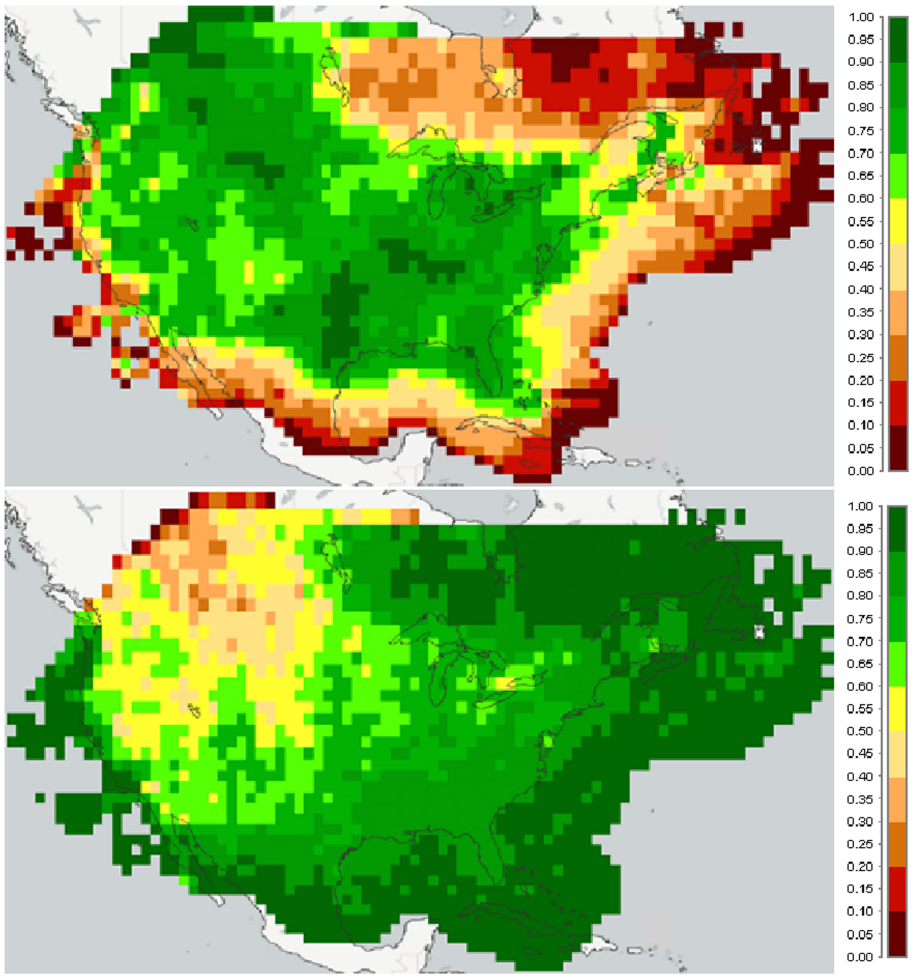

Figure 3. (a) Upper bound on the total lightning DE of the NLDN, $\frac{P(N)}{P(N \cup G)}$ according to equation (5). The same color scale as in Figure 2a applies. (b) Upper bound on the total lightning DE of the GLM, $\frac{P(G)}{P(N \cup G)}$, according to equation (4). The same color scale as in Figure 2a applies.

In broad terms, on average, oceanic lightning is more intense than continental lightning. In the case of CGs, the prior literature shows higher peak current over ocean in the case of first strokes in negative CG flashes (e.g., Cummins et al., 2005; Orville et al., 2011), but not subsequent strokes or positive CG strokes. Chronis et al. (2016) explores the phenomenology of higher oceanic peak currents and includes a number of confounding factors. With respect to ICs, the literature does not mention the effective peak currents of IC events reported by ground-based LLS data. However, the LIS and OTD data presented by Beirle et al. (2014) show more groups per flash, events per flash, and higher radiance from oceanic lightning, suggesting that oceanic ICs may in fact be more intense.

One of the factors discussed by Chronis et al. (2016) is the effective ice particle size at cloud top from MODIS (Moderate Resolution Imaging Spectroradiometer). The monthly/1° time-space climatology of this field shows good consistency (though not perfect) with the −CG peak current amplitude time-space variability. The effective ice crystal size at cloud top might reasonably be expected to relate to optical thickness, and thus GLM DE. Figure 10 of Chronis et al. (2016) show a distinct land-ocean contrast in effective ice crystal size. But, over land areas, its pattern is not consistent with the pattern of GLM DE. For example, in places where GOES-17 has high relative DE (like CA, NV, and AZ), the effective ice crystal size is just as small as in places where both GLMs have relatively low DE (e.g., CO, WY, and NM). Further to the question of optical thickness, Figure 10 of Stolz et al. (2015) shows that at any particular flash density, the 30 dBz echo altitude is roughly equivalent across both oceanic and continental storms. To the extent that vertical profile of reflectivity might serve as a (crude) optical depth proxy, then Stolz's result indicates that oceanic and

21698996, 2020, 5, Downloaded from https://agupubs.onlinelibrary.wiley.com/doi/10.1029/2019JD031172 by Capes, Wiley Online Library on [01/10/2025]. See the Terms and Conditions (https://onlinelibrary.wiley.com/terms-and-conditions) on Wiley Online Library for rules of use; OA articles are governed by the applicable Creative Commons License

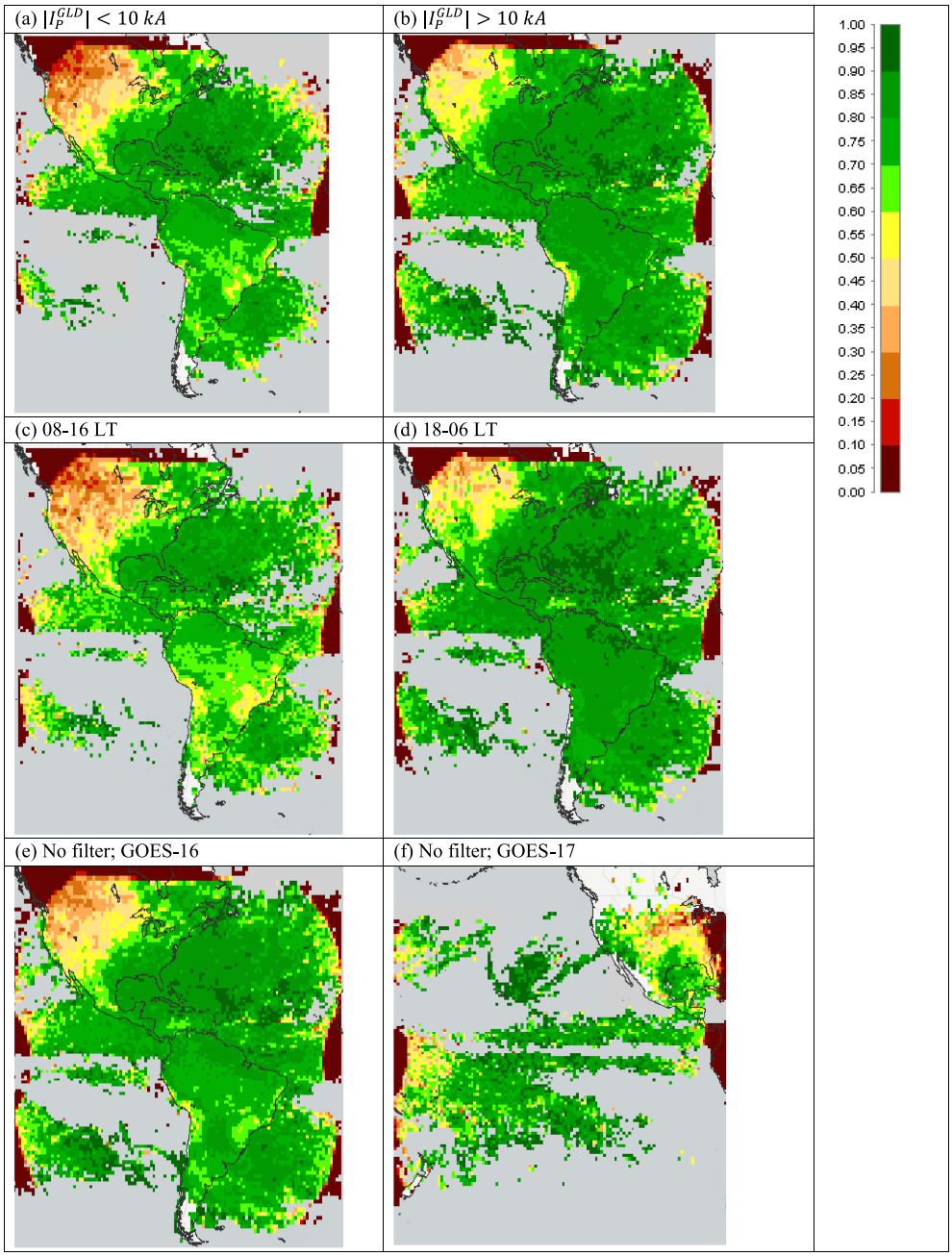

Figure 4. Conditional flash detection efficiencies, P (GLM|GLD360), on a 1° × 1° grid. Pixels with fewer than 100 reference events are omitted. (a–e) GOES-16 DE evaluated between 2018-02-13 and 2019-04-01. (f) GOES-17 DE evaluated between 2019-02-08 and 2019-05-01. (a–d) The conditional DE with the reference data filtered according to peak current magnitude (a and b) and local time range (c and d). All plots use the color scale shown on the right. Please note that areas in dark red around edges are outside the GLM field of view.

continental storms are equally optically thick given the same amount of lightning. However, since the frequency with which any given lightning flash density occurs over ocean is much lower, on average oceanic storms could still be less optically thick than continental storms.

Beyond the dependencies on flash energetics and optical depths, the patterns of high and low GLM DE in Figure 4 do not exactly align with coastlines, nor do they align exactly with day-night tendencies. The GOES-16 GLM low DE region extends well into the plains, where there is a tendency toward nocturnal storms (Holle, 2014) that should be more easily detected. But there is also an inverse relationship between

21698996, 2020, 5, Downloaded from https://agupubs.onlinelibrary.wiley.com/doi/10.1029/2019JD031172 by Capes, Wiley Online Library on [01/10/2025]. See the Terms and Conditions (https://onlinelibrary.wiley.com/terms-and-conditions) on Wiley Online Library for rules of use; OA articles are governed by the applicable Creative Commons License

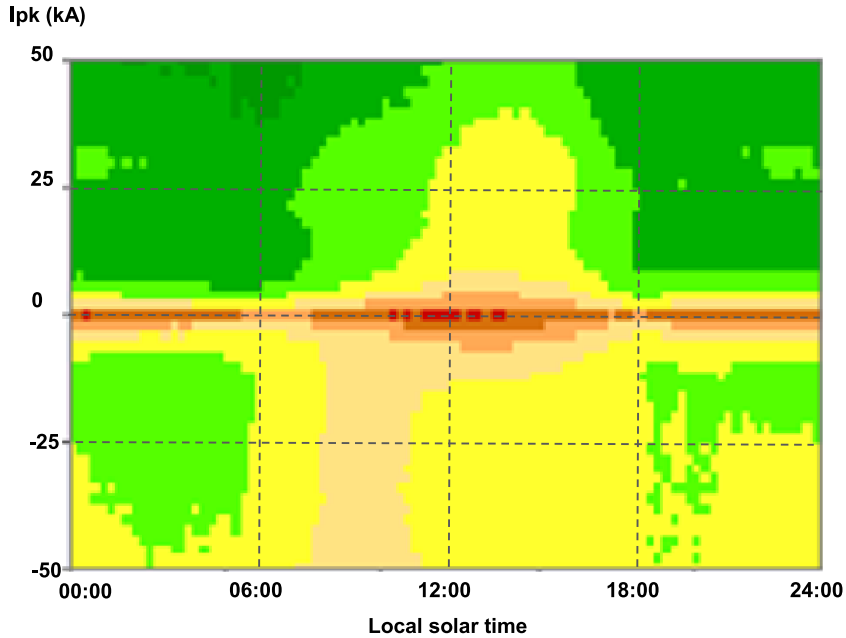

Figure 5. Relative group DE P (GLM group|GLD360) plotted against GLD360-determined peak current (*y* axis) and LST (*x* axis).

the amount of CG lightning and the geometric mean peak current of first strokes (Chronis, Cummins, et al., 2015). This dependency might suggest lower GLM DE, even though the storms are more frequently nocturnal (and the peak current variation in Chronis, Cummins, et al., 2015, is only about 3–5 kA between the low and high points). Additionally, the GOES-17 GLM has high DE over the Gulf of Mexico, but it also has high DE a few hundred km into the south-central United States before it drops off farther inland. Additionally, the inland portions of the southeast and south-central United States have a strong afternoon peak in lightning, but yet they still have high GLM DE.

Comparing Figures 4e to 4f shows an apparent additional factor: the incidence angle at the GLM sensor. GOES-17 has a much higher DE over the western edge of the United States but falls off on the northeast corner of its field of view, where GOES-16 has a relatively higher DE. Thus, Figure 4 encapsulates a very complicated mix of factors that clearly need to be deconvolved in future research.

Figure 5 summarizes the significant dependence of DE on both peak current and LST, showing the conditional GLM group DE of GOES-16 plotted against peak current and LST. The fact that GLM detects more positive strokes than negative strokes suggests an optical depth component. Weak positive strokes, for example, are likely to be associated with cloud pulses in normally electrified storms and would presumably have a shorter optical depth to the cloud top compared to weak negative return strokes or negative cloud pulses in anomalously electrified storms.

3.2. Analysis of GLM DE—Small, Isolated Storms Over Western United States

Large-scale analyses can mask details in a variety of ways, for example, by mixing storms of high and low flash rates and storms of different morphology (e.g., severe storms, mesoscale convective systems, and ordinary air mass storms), lightning characteristics, and cloud optical properties. In order to try to clarify the inferred total lightning DE upper bounds of both the GOES-16 GLM and the NLDN over the western United States, we have selected a number of small, isolated, air mass storms over the western United States with low flash rates and performed flash-level comparisons manually. Low flash rate storms completely eliminate the problem of flash clustering differences between the two systems, and our selection of storms that are small and isolated in space also eliminates any potential confounding issues of misassociation of flashes from neighboring storm cells. This analysis effectively provides a “microscope-level” view into the question of what is detected by each system.

21698996, 2020, 5, Downloaded from https://agupubs.onlinelibrary.wiley.com/doi/10.1029/2019JD031172 by Capes, Wiley Online Library on [01/10/2025]. See the Terms and Conditions (https://onlinelibrary.wiley.com/terms-and-conditions) on Wiley Online Library for rules of use; OA articles are governed by the applicable Creative Commons License

Table 2
Isolated Air Mass Storms Over the Western United States as Detected by the GOES-16 GLM and the NLDN

Date/time	Town/city	GLM flashes	NLDN flashes	$P(N\|G)$	$P(G\|N)$
2018-05-29 00:00–00:45	Elko, NV	23	19	0.696	0.842
2018-06-03 19:35–20:40	Blackhawk, CO	48	45	0.396	0.422
2018-06-06/07 23:45–01:40	Reno, NV	61	64	0.311	0.312
2018-06-10 20:50–23:50	Elk City, ID	7	6	0.571	0.667
2018-06-11 20:55–21:15	Ovando, MT	1	5	1.000	0.200
2018-06-14 14:30–15:25	Green River, UT	9	10	0.778	0.700
2018-06-15 22:10–23:00	Mountain Home, UT	9	9	0.444	0.444
2018-06-18 18:55–23:30	Jackpot, NV	47	65	0.766	0.600
2018-06-20 01:15–01:50	Steamboat Sprs, CO	8	9	0.750	0.667
	Total	213	232	0.521	0.500

Note. The nearest town/city is given as a general indication of the location of the storms, each of which covered an area less than or equal to about 25 × 25 km^2. All times are in UTC.

Table 2 lists the selected storm cases, their approximate locations, the numbers of flashes observed by both the GOES-16 GLM and the NLDN, and the two conditional probabilities, $P(N|G)$ and $P(G|N)$. The summary line at the bottom indicates that only about half of each system's flashes are matched by the other system, so there is a population of flashes that each system detects that the other system misses. In the case of NLDN, with regard to total lightning, this is expected: The NLDN cloud flash DE has been validated against LMAs (Murphy & Nag, 2015) and found to be between 50% and 60%, while the CG flash DE of NLDN is around 95% (Zhu et al., 2016, and references therein). If cloud flashes make up approximately 75% of all lightning flashes, then the overall total lightning DE of NLDN should be expected to be approximately 0.75(0.55) +0.25(0.95) = 0.65 The GLM, on the other hand, was originally expected to detect 70–90% of total lightning (Goodman et al., 2013). By applying the Bayesian method of Bitzer and Burchfield (2016) to the values of $P(N|G)$ and $P(G|N)$ at the bottom of Table 2, we find that the upper bound on the total lightning DE of NLDN, $P(N)$, given this sample of small storms over the western United States, is 0.70, whereas the upper bound on the GLM's DE, $P(G)$, is 0.66. It appears, then, that the GOES-16 GLM may actually have a slightly lower total lightning DE than NLDN over the western U.S.

3.3. Severe Storm Cases: Lightning Jump Statistics

Table 3 shows the numbers of storms tracked in each of the five severe storm cases (see section 2), the number of lightning jumps produced by the NLDN, GLM, and the number of lightning jumps that either overlapped in time between NLDN and GLM or whose start times differed by no more than the update time of the storm tracking method, which is 2 min ("match"). Most of the NLDN and GLM lightning jumps do not match by this definition: The percentages of matching jumps vary widely, with a minimum of less than 7% in the 2018-07-29 case over Wyoming and Colorado to a maximum of almost 43% in the 2018-08-17 case near the east coast. The greatest disparity in jump matching between the NLDN and GLM with like storm morphology is between the two cases of supercell storms: the 2018-07-29 and 2018-07-19 cases, where the latter has a much higher percentage of matched lightning jumps than the former. Thus, the supercell cases are used to start a more detailed look at the severe storm cases.

3.4. Severe Storm Cases: Supercells

Figures 6 and 7 present two sets of nearby pairs of storms. Figure 6 is from the 2018-07-29 case, where two storms were located near Laramie, Wyoming, at 23:40 UTC. Figure 7 is from the 2018-07-19 case, with two storms near Des Moines, Iowa. In each figure, the top and middle panels show the flash rates, with NLDN shown in blue and GLM shown in orange. Lightning jumps are indicated in red. At the bottom of each figure is a plot of the radar reflectivity and GLM group data, in the same form presented in Figure 1 above. The storm track positions are also shown in the bottom panels, although these are not relevant to the discussion.

Table 3
Lightning Jump Statistics by Date

Date	Storms	NLDN LJ	GLM LJ	Match	% NLDN LJ matched
2018-06-19	6	14	13	4	28.6
2018-07-19	6	20	25	7	35.0
2018-07-29	12	44	25	3	6.8
2018-08-17	12	28	19	12	42.9
2018-08-27	11	25	33	10	40.0
All	47	131	120	36	27.5

Both of these cases were determined to be supercell cases by examination of the 00:00 UTC soundings at downstream stations (00:00 on 2018-07-30 at Denver, Colorado, in the case of Figure 6 and 00:00 on 2018-07-20 at Davenport, Iowa, in the case of Figure 7). Thompson et al. (2004a) defined a "supercell composite parameter" (SCP) on the basis of the most unstable CAPE, effective bulk wind difference, and effective storm-relative helicity. The definitions of "effective" are described in detail by the Thompson et al. group (Thompson et al., 2003; Thompson et al., 2004; Thompson et al., 2004b; Thompson et al., 2012; Thompson, Edwards, & Mead, 2004a) but essentially have to do with the inflow corresponding to the most unstable parcel in the lower troposphere. Based on sounding data, rather than NWP data, we have approximated the effective layers as the

21698996, 2020, 5, Downloaded from https://agupubs.onlinelibrary.wiley.com/doi/10.1029/2019JD031172 by Capes, Wiley Online Library on [01/10/2025]. See the Terms and Conditions (https://onlinelibrary.wiley.com/terms-and-conditions) on Wiley Online Library for rules of use; OA articles are governed by the applicable Creative Commons License

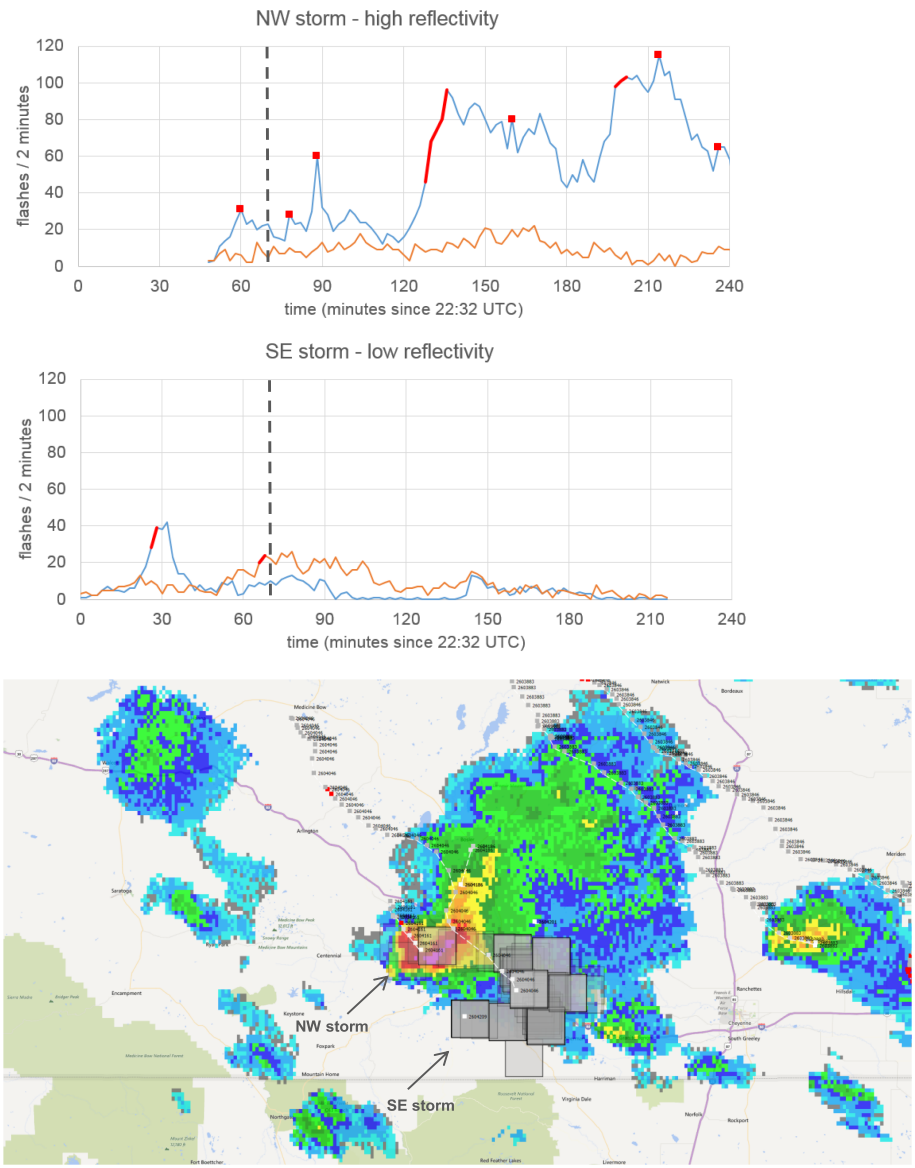

Figure 6. Top and middle: NLDN flash rate (blue) and GLM flash rate (orange) and lightning jumps (red) versus time. Bottom: radar and GLM groups, as in Figure 1, at 23:40 UTC on 2018-07-29, 68 min into the time series plots in the top and middle panels. The northwestern storm of this pair, with high reflectivity, is shown in the top panel, and the southeastern storm, with lower reflectivity, is in the middle panel. The 68-min point is marked by the dashed lines in the top and middle panels.

0–2 km AGL layer in the case of storm-relative helicity, and in the case of bulk wind difference, the layer from 885 to 469 hPa in the 2018-07-20 Davenport sounding and from 840 to 399 hPa in the 2018-07-30 Denver sounding. With that, we obtain SCP values of 9.26 (Davenport, 2018-07-20) and 10.72 (Denver, 2018-07-30). Both of those values are well within the midrange of values that Thompson et al. (2003) attribute to "significant tornado" storms.

As shown in Figure 6, there is no correlation whatsoever between the NLDN and GLM flash rates in the northwestern storm of the selected storm pair, where the reflectivity values are extremely high. The NLDN exhibited higher flash rates than GLM by up to a factor of 6 in this storm, and the NLDN also produced the only lightning jumps found in this storm. The GLM, by contrast, showed a nearly flat flash rate during the entire life cycle of this storm. The storm to the southeast produced much lower flash rates

21698996, 2020, 5, Downloaded from https://agupubs.onlinelibrary.wiley.com/doi/10.1029/2019JD031172 by Capes, Wiley Online Library on [01/10/2025]. See the Terms and Conditions (https://onlinelibrary.wiley.com/terms-and-conditions) on Wiley Online Library for rules of use; OA articles are governed by the applicable Creative Commons License

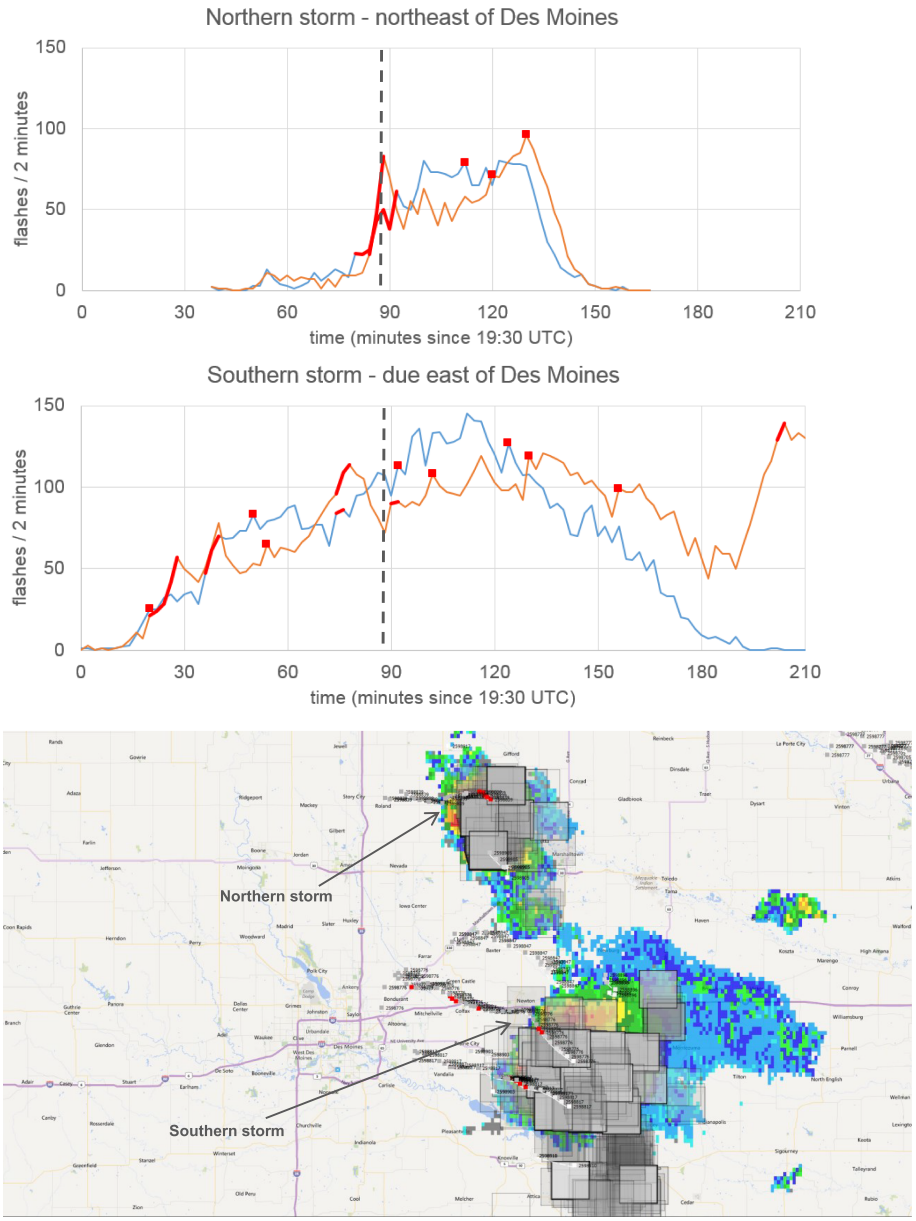

Figure 7. Top and middle: NLDN flash rate (blue) and GLM flash rate (orange) and lightning jumps (red) versus time. Bottom: radar and GLM groups, as in Figure 1, at 20:58 UTC on 2018-07-19, 88 min into the time series plots in the top and middle panels. The northern storm of this pair, near the top of the bottom panel, is shown in the top panel, and the southern storm, due east of Des Moines, Iowa, is in the middle panel. The 88-min point is marked by the dashed lines in the top and middle panels.

overall than the northwestern storm, and aside from a major peak in NLDN flash rate near the start of this storm, the NLDN and GLM flash rates were relatively better correlated in the southeastern cell.

Figure 7 is from the Iowa storms on 2018-07-19. The middle panel refers to the storm that is essentially due east of Des Moines; this storm has another nearby neighbor just to its south, but that storm is not considered in this cell-to-cell comparison. Note that the NLDN and GLM flash rates are very well correlated in both of the cells shown in Figure 7, except after the 180-min mark of the southern storm. That later deviation of the NLDN and GLM flash rates appears to be a noticeable exception to the comment above regarding the assignment of GLM flashes to NLDN-base storm tracks: Namely, the close proximity of the two nearby cells toward the end of the life cycle causes GLM flashes from the nearby neighbor of the southern storm to be associated

21698996, 2020, 5, Downloaded from https://agupubs.onlinelibrary.wiley.com/doi/10.1029/2019JD031172 by Capes, Wiley Online Library on [01/10/2025]. See the Terms and Conditions (https://onlinelibrary.wiley.com/terms-and-conditions) on Wiley Online Library for rules of use; OA articles are governed by the applicable Creative Commons License

with the storm of interest. The generally excellent correlation between NLDN and GLM flash rates in both of the Iowa cells contrasts significantly with the northwestern storm of the Wyoming storm pair in Figure 6. Additionally, note that the lightning jumps in the NLDN and GLM flash rate time series are also much better correlated in the Iowa storms than in the Wyoming storms in Figure 6.

Both the 2018-07-19 and 2018-07-29 cases have the supercell mode of organization, so storm morphology cannot be primarily responsible for the vast difference in GLM flash rate behavior relative to NLDN. The total flash rates in the Iowa storms actually peak at slightly higher values than either Wyoming storm, so a high flash rate by itself is not an explanation of the discrepancies either.

3.5. Severe Storm Cases: Linear/Cluster Storms

Figure 8 shows a pair of storms in a quasi-linear system to the northwest of Philadelphia. Earlier in the lifetime of the northern storm, its NLDN, and GLM flash rates are much better correlated, but most of that time corresponds to when the storm was relatively isolated. Between about 22:20 and 23:30, however, its flash rates are rather poorly correlated. At 22:50, the GLM has just reported a lightning jump in this storm, but the NLDN flash rate is lower and in decline. Earlier in this storm, the NLDN had a jump. Conversely, the southern storm has nicely correlated flash rates at this time. The NLDN is in the middle of a jump at 22:50, but the GLM is not, although it is in the middle of a nonjump increase in flash rate. Recall that Schultz et al. (2017) showed that lightning jumps and nonjump increases in flash rate are associated with statistically significant differences in peak updraft speed and the volume of updraft $\geq$10 m/s. However, it is also critical to recall that those results are all based on LMA data. Here, the lightning jumps and nonjump flash rate increases are not observed by LMAs, and it seems likely that the Schultz et al. (2017) results may have to be revisited when the lightning observing system is not an LMA, simply because of the differences in observation characteristics and flash clustering algorithms.

Figure 9 shows another set of storms near the south end of the Minnesota storm line near 23:30 UTC on 2018-08-27. In contrast to Figure 8, the GLM and NLDN flash rates are poorly correlated over the entire storm track durations. At the specific time of interest in Figure 9, 23:30 UTC, the GLM flash rate in the northern storm is roughly twice that of NLDN and is nearly flat while the NLDN flash rate is dropping slightly. The southern storm is nearly the opposite—NLDN has about twice the flash rate of GLM, but the trend is similar (NLDN dropping, GLM nearly flat). In neither storm do the jumps match well at all.

3.6. ABI and Radar Data

ABI attributes of all storms in Figures 6–9 are examined within a radius of 20 km of the NLDN-derived storm tracks. The selected ABI attributes are the maximum cloud top altitude, minimum Channel 7 BT, and maximum RRQPE value within 20 km of the NLDN-derived storm tracks. The ABI cloud top altitude and channel 7 BT update once every 5 min over the CONUS sector, while the RRQPE field updates every 15 min. The storm tracks update every 2 min, so the ABI attributes of the selected storms change only when either (a) a new 5- or 15-min ABI update is available, or (b) the storm track moves sufficiently to pick up new ABI grid boxes that are within 20 km and at least one of those new grid boxes contains a higher maximum (or lower minimum) of one of the selected ABI fields.

In general, across both supercell and linear storm cases, the maximum cloud top altitude and minimum Channel 7 BT exhibit little variation as a function of time through the life cycles of the storms in Figures 6–9, and they almost never show much correlation with the lightning flash rates (hence, not shown). The primary variation in the Channel 7 BT is its overall tendency to decrease as sunset approaches and the background surface-based emission begins to change.

The only ABI field that does correlate somewhat with flash rate is the maximum RRQPE. That modest correlation is subject, however, to the update rate issue just mentioned above, as well as the fact that the RRQPE saturates at 48 mm/hr. The modest tendency of the RRQPE to correlate with the lightning data suggests that actually radar, which obviously updates more frequently and has higher resolution than RRQPE, would provide more useful information than the ABI RRQPE field. Figure 10 presents a series of comparisons of vertical profiles of reflectivity from radar and key parameters from ABI: the maximum cloud top altitude and the minimum Channel 7 BT translated to altitude by way of the nearest sounding. Each comparison is made at the time of the vertical dashed lines from Figures 6–9, namely, 23:40 UTC on 2018-07-29 in the Wyoming

21698996, 2020, 5, Downloaded from https://agupubs.onlinelibrary.wiley.com/doi/10.1029/2019JD031172 by Capes, Wiley Online Library on [01/10/2025]. See the Terms and Conditions (https://onlinelibrary.wiley.com/terms-and-conditions) on Wiley Online Library for rules of use; OA articles are governed by the applicable Creative Commons License

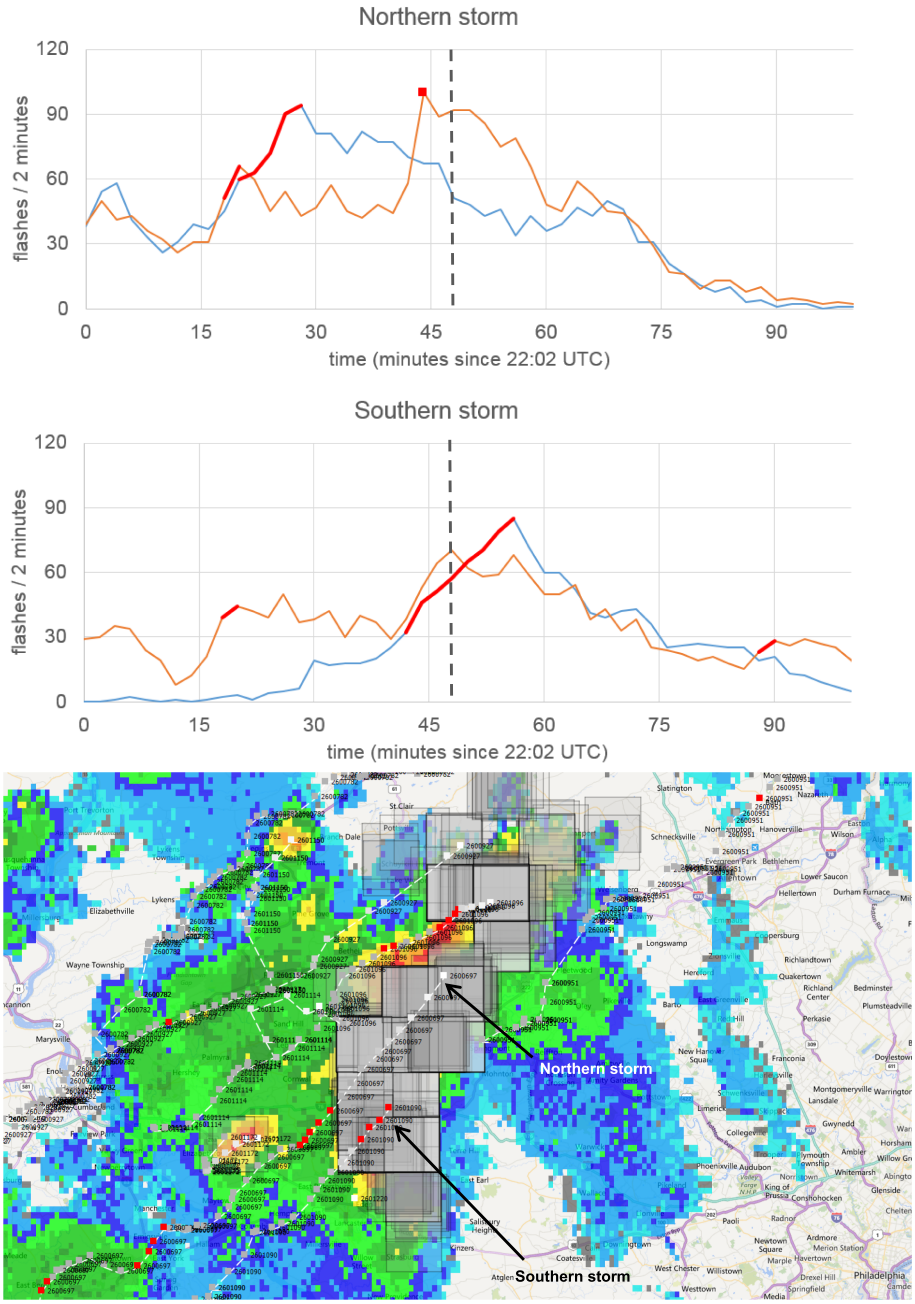

Figure 8. Top and middle: NLDN flash rate (blue) and GLM flash rate (orange) and lightning jumps (red) versus time. Bottom: radar and GLM groups, as in Figure 1, at 22:50 UTC on 2018-08-17, 48 min into the time series plots in the top and middle panels. This line of storms is northwest of Philadelphia. The northern storm of this pair, near the top of the bottom panel, is shown in the top panel, and the southern storm is in the middle panel. The 48-min point is marked by the dashed lines in the top and middle panels.

storms (Figure 6), 20:58 UTC on 2018-07-19 in the Iowa storms (Figure 7), 22:50 UTC on 2018-08-17 in the storms near Philadelphia (Figure 8), and 23:30 UTC on 2018-08-27 in the Minnesota storms (Figure 9).

The top part of Figure 10 contrasts two of the supercells: the northwestern storm from the pair near Laramie, Wyoming, from Figure 6 and the storm just east of Des Moines, Iowa, from Figure 7. Recall that in the former case, the NLDN has much higher flash rates than GLM at almost all times throughout the storm, while the GLM flash rate is low and nearly flat. In the Iowa storm, by contrast, the NLDN and GLM flash rates are very well correlated, and the lightning jumps also match reasonably well. The most significant difference

21698996, 2020, 5, Downloaded from https://agupubs.onlinelibrary.wiley.com/doi/10.1029/2019JD031172 by Capes, Wiley Online Library on [01/10/2025]. See the Terms and Conditions (https://onlinelibrary.wiley.com/terms-and-conditions) on Wiley Online Library for rules of use; OA articles are governed by the applicable Creative Commons License

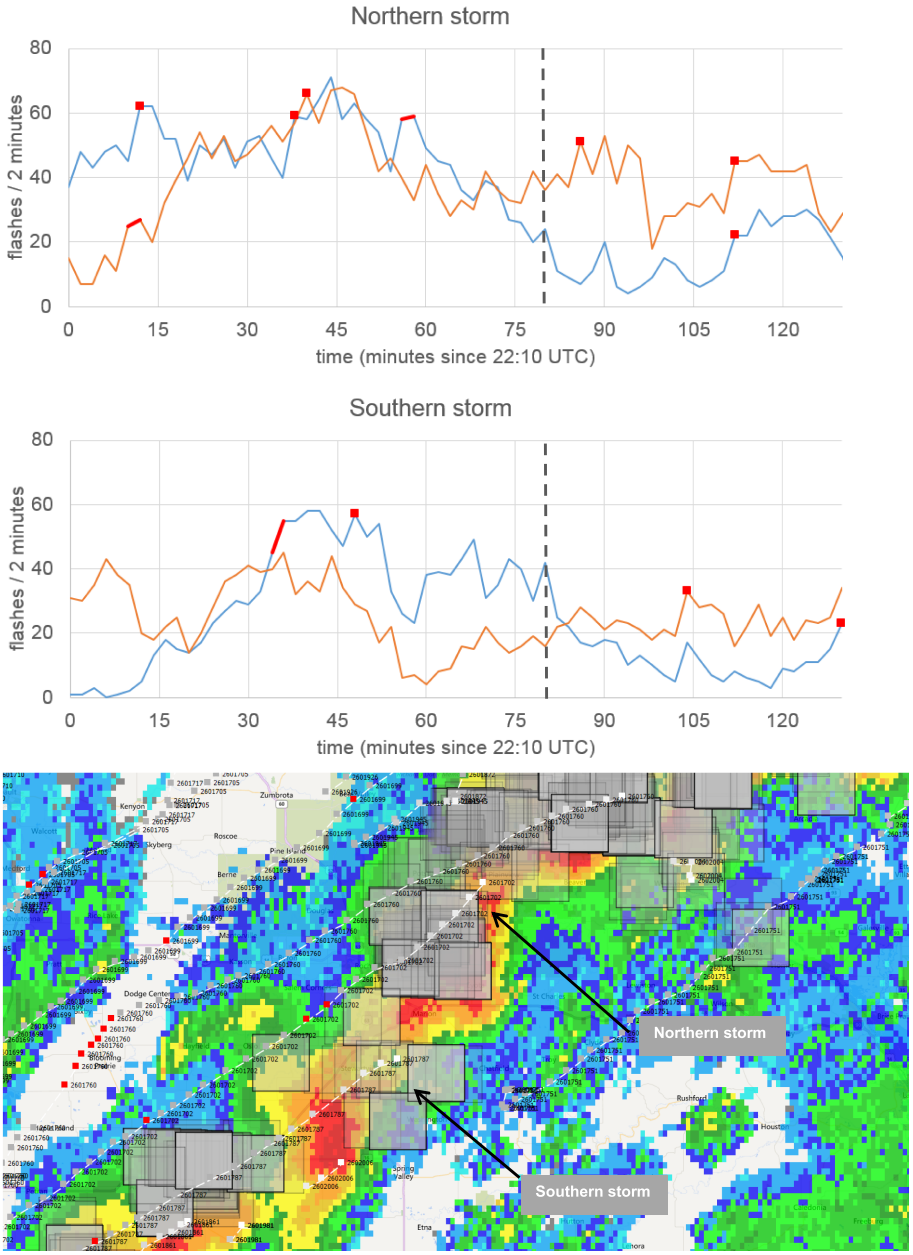

Figure 9. Top and middle: NLDN flash rate (blue) and GLM flash rate (orange) and lightning jumps (red) versus time. Bottom: radar and GLM groups, as in Figure 1, at 23:30 UTC on 2018-08-27, 80 min into the time series plots in the top and middle panels. This line of storms is over southern Minnesota. The northern storm of this pair, near the top of the bottom panel, is shown in the top panel, and the southern storm is in the middle panel. The 80-min point is marked by the dashed lines in the top and middle panels.

between these two storms is obviously the vertical profile of reflectivity. The ABI actually shows a higher cloud top altitude, by 1 km, in the Iowa storm, as well as a higher effective altitude of the Channel 7 emissions, but yet the GLM detects an order of magnitude higher lightning flash rate in the Iowa storm compared to the Wyoming storm and is, moreover, very well correlated with NLDN.

The dearth of GLM flashes from the Wyoming storm might be explained partially by its location, given our analysis of the relatively low flash DE of GLM over the western United States. However, in addition, one or both of the following factors could also be involved: (a) The storm could be anomalously electrified (Bruning et al., 2014), with more cloud flashes originating at lower altitudes than in the Iowa storm (Fuchs &

21698996, 2020, 5, Downloaded from https://agupubs.onlinelibrary.wiley.com/doi/10.1029/2019JD031172 by Capes, Wiley Online Library on [01/10/2025]. See the Terms and Conditions (https://onlinelibrary.wiley.com/terms-and-conditions) on Wiley Online Library for rules of use; OA articles are governed by the applicable Creative Commons License

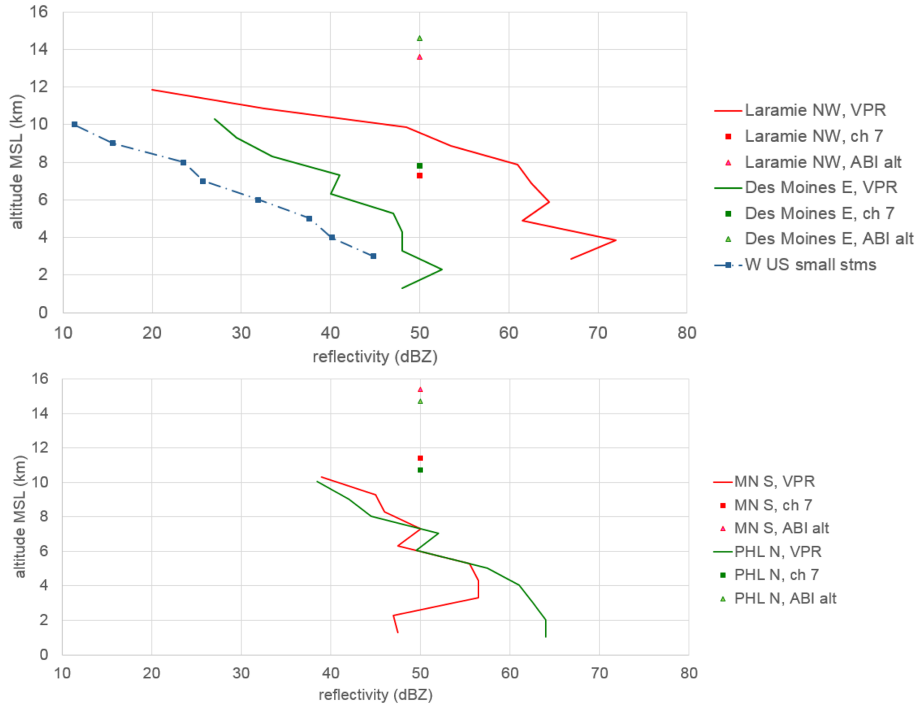

Figure 10. Vertical profiles of reflectivity and altitude points corresponding to key ABI attributes. The top panel compares two of the supercell cases, the northwestern storm from the pair near Laramie, Wyoming, from Figure 6 and the storm east of Des Moines, Iowa, from Figure 7. The top panel also shows the average vertical profile of reflectivity from the isolated western U.S. storm cases discussed in section 3.2. The bottom panel compares two storms from the linear cases, the northern storm from the pair near Philadelphia from Figure 8 and the southern storm from the Minnesota line from Figure 9. The ABI altitudes are plotted as points at the 50-dBZ point on the horizontal axis. Triangles show the ABI cloud top altitude, and squares show the altitude corresponding to the Channel 7 brightness temperature, taken from the nearest proximity sounding.

Rutledge, 2018), and/or (b) the storm could simply be more optically thick than the Iowa storm. The former question is not addressed directly, due to a lack of LMA data but rather by an examination of the polarities of cloud pulses and CG strokes detected by the NLDN. The majority of cloud pulses are of positive polarity at 23:40 UTC (a condition that persisted, in fact, until after 00:30 UTC). As well, although CG flashes are vastly outnumbered by cloud flashes in this storm, over 60% of all CG strokes with peak currents above 15 kA (absolute value) are negative. These are precisely the polarities observed in normally electrified, ordinary air mass thunderstorms. Thus, while the available data do not allow us to rule out anomalous electrification, it appears that the leading explanation of the discrepancy between the Wyoming and Iowa supercell cases is optical thickness, based on the major contrast between their vertical profiles of reflectivity in Figure 10. Thomas et al. (2019) noted that the absorption of near-IR signals by H_2O (of any phase) can become very significant as the path length increases and the number and sizes of particles (and thus radar reflectivity) increase.

The top panel of Figure 10 also shows the average of the vertical profiles of reflectivity from seven of the isolated western U.S. storms that are discussed in section 3.2. These seven storms were within reasonable distance of the nearest radar (the others were not) such that vertical profiles of reflectivity were readily observed over most of the depth of the storms. Note that the average profile from these seven storms consists of lower reflectivity at all altitudes than the Iowa supercells (never mind the Laramie supercell), but yet recall that the relative DE of GLM in these storms was also quite low. Thus, the optical depth of these western U.S. isolated storms probably does not explain the relatively low DE, suggesting perhaps other issues. One candidate might be off-boresight effects (Boccippio et al., 2002), in combination with some other issue that affects land-based but not oceanic lightning; recall that Figures 4e and 4f only show significantly reduced DE over land. Another candidate could be small flash size or short flash duration (Zhang & Cummins, 2019). These particular western U.S. storms are not within range of any LMA, but in the future, storms that are close to an

21698996, 2020, 5, Downloaded from https://agupubs.onlinelibrary.wiley.com/doi/10.1029/2019JD031172 by Capes, Wiley Online Library on [01/10/2025]. See the Terms and Conditions (https://onlinelibrary.wiley.com/terms-and-conditions) on Wiley Online Library for rules of use; OA articles are governed by the applicable Creative Commons License

LMA (such as that near Ft. Collins, Colorado) could be used to investigate whether small flash size and/or short duration in small, isolated, western U.S. storms is indeed a significant factor behind the low GLM DE in such cases.

Two of the storms from the linear/cluster cases are presented in the lower part of Figure 10: the northern storm from the Philadelphia pair from Figure 8 and the southern storm from the Minnesota storm pair from Figure 9. At the selected times in Figures 8 and 9, respectively, the Philadelphia case has roughly twice as high a GLM flash rate as its NLDN flash rate, while the exact opposite is true of the Minnesota storm. These storms have essentially identical vertical profiles of reflectivity from 5 km up and virtually identical ABI-identified cloud top altitudes as well as the effective altitude of the Channel 7 emission. In addition, both storms are dominated by positive-polarity cloud pulses and negative CG flashes (though outnumbered by cloud flashes in both cases), suggesting normal electrification. Neither of these storms has high flash rates in comparison to the Iowa supercells or the northwestern supercell from the Wyoming pair. Yet neither of these storms has great correlation between the GLM and NLDN flash rates either, especially when viewed in comparison to the two Iowa supercells where the correlation is significantly better. This suggests possible factors such as the obviously different methods of flash clustering between NLDN and GLM, or the method of association of GLM flashes to the NLDN-based storm tracks, or some combination of these with detection efficiency effects such as those described by Zhang and Cummins (2019).

4. Conclusions

In this study, we have analyzed the relative performance of the GLMs on the GOES-16 and -17 satellites with respect to the NLDN and GLD360 and have demonstrated that the GLM DE falls off substantially over the landmass of the United States within about 2,000 km of the edge of the field of view of each GLM. Thus, the GOES-16 GLM is the instrument of preference from the Great Plains eastward, while the GOES-17 GLM appears to be preferable over the western United States.

The spatial and temporal DE dependencies depend on a combination of a variety of factors, including flash size, total optical depth, optical power, time of day, and incidence angle at the GLM sensor. In addition, the degree to which GLM and ground-based LLSs detect different subsets of flashes or processes within flashes certainly warrants future research. With these confounding factors in mind, we find that the DE falls off most rapidly on the northwest and northeast corners of the GOES-16 and -17 fields of view, respectively, over a region where thunderstorms occur over land, typically in the late afternoon. Such storms are generally characterized by lower peak current magnitudes on average and likely higher reflectivity at midaltitudes and upper altitudes than their oceanic counterparts. These broad spatial and temporal patterns provide the backdrop of our analyses of individual storms.

The first set of individual storm cases consisted entirely of small, isolated storms with very low lightning flash rates over the western United States, with GLM data from GOES-16. These storms all exhibited characteristics of normal electrification, with entirely negative CG flashes and cloud pulses of almost entirely positive polarity. The vertical profiles of reflectivity in these isolated storms show lower reflectivity at middle and high altitudes than any of the severe storm cases, suggesting that the optical depth of the cloud between the lightning and cloud top should not have been a factor in the relatively low DE of the GLM. The small sizes and isolated nature of these storms could indicate that the flashes themselves may have been fairly small in size and/or of short duration. If that is the case, it would suggest reduced GLM DE, consistent with Zhang and Cummins (2019).

In a selected set of severe storms, the GLM and NLDN flash rates were found to vary widely in their relationship to one another, even when factors such as storm morphology and storm location are controlled. The ABI fields Channel 7 BT and cloud top altitude appear to be of little use in terms of assessing why GLM does or does not correlate well with NLDN. The vertical profile of reflectivity, however, differs dramatically between the selected supercell cases in this analysis. This suggests that high optical thickness associated with heavy midlevel precipitation is a dominant factor in modulating the DE of GLM. In the selected linear/clustered storms in this study, there is almost no difference in vertical profile of reflectivity or ABI properties. Thus, some combination of flash clustering differences and overlap of the GLM-storm track assignment radii (as used in this analysis) between neighboring storm cells probably influences the GLM-NLDN flash rate relationship in these storms. In such situations, it may be preferable to vary GLM-

21698996, 2020, 5, Downloaded from https://agupubs.onlinelibrary.wiley.com/doi/10.1029/2019JD031172 by Capes, Wiley Online Library on [01/10/2025]. See the Terms and Conditions (https://onlinelibrary.wiley.com/terms-and-conditions) on Wiley Online Library for rules of use; OA articles are governed by the applicable Creative Commons License

to-storm track assignment radii according to the distances between neighboring storm tracks as given by NLDN.

Acknowledgments
GOES-16 and -17 GLM and ABI data can be obtained from the NOAA CLASS (Comprehensive Large Array data Stewardship System) site (https://www.avl.class.noaa.gov/saa/products/welcome;jsessionid=

References

Beirle, S., Koshak, W., Blakesless, R., & Wagner, T. (2014). Global patterns of lightning properties derived by OTD and LIS. *Natural Hazards and Earth System Sciences*, *14*, 2715–2726. https://doi.org/10.5194/nhess-14-2715-2014

Bitzer, P. M., & Burchfield, J. C. (2016). Bayesian techniques to analyze and merge lightning locating system data. *Geophysical Research Letters*, *43*. https://doi.org/10.1002/2016GL071951

Boccippio, D. J., Koshak, W. J., & Blakeslee, R. J. (2002). Performance assessment of the Optical Transient Detector and Lightning Imaging Sensor. Part I: Predicted diurnal variability. *Journal of Atmospheric and Oceanic Technology*, *19*, 1318–1332.

Bruning, E. C., & MacGorman, D. R. (2013). Theory and observations of controls on lightning flash size spectra. *Journal of the Atmospheric Sciences*, *70*, 4012–4029.

Bruning, E. C., Weiss, S. A., & Calhoun, K. M. (2014). Continuous variability in thunderstorm primary electrification and an evaluation of inverted-polarity terminology. *Atmospheric Research*, *135-136*, 274–284.

Chronis, T., Carey, L. D., Schultz, C. J., Schultz, E. V., Calhoun, K. M., & Goodman, S. J. (2015). Exploring lightning jump characteristics. *Weather and Forecasting*, *30*, 23–37.

Chronis, T., Cummins, K., Said, R., Koshak, W., McCaul, E., Williams, E. R., et al. (2015). Climatological diurnal variation of negative CG lightning peak current over the continental United States. *Journal of Geophysical Research*, *120*, 582–589. https://doi.org/10.1002/2014JD022547

Chronis, T., Koshak, W., & McCaul, E. (2016). Why do oceanic negative cloud-to-ground lightning exhibit larger peak current values? *Journal of Geophysical Research*, *121*, 4049–4068. https://doi.org/10.1002/2015JD024129

Cummins, K. L., Cramer, J. A., Brooks, W. A., & Krider, E. P. (2005). On the effect of land:sea and other Earth surface discontinuities on LLS-inferred lightning parameters, Paper presented at VIII International Symposium on Lightning Protection (SIPDA), University of Sao Paulo, Sao Paulo, Brazil.

Curtis, N., Carey, L. D., & Schultz, C. J. (2018). An analysis of the lightning jump algorithm using Geostationary Lightning Mapper flashes, Paper presented at 25th International Lightning Detection Conference and 7th International Lightning Meteorology Conference, Vaisala Inc., Ft. Lauderdale, FL.

Farnell, C., Rigo, T., & Pineda, N. (2017). Lightning jump as a nowcast predictor: Application to severe weather events in Catalonia. *Atmospheric Research*, *183*, 130–141.

Fuchs, B. R., & Rutledge, S. A. (2018). Investigation of lightning flash locations in isolated convection using LMA observations. *Journal of Geophysical Research*, *123*, 6158–6174. https://doi.org/10.1002/2017JD027569

Gatlin, P. N., & Goodman, S. J. (2010). A total lightning trending algorithm to identify severe thunderstorms. *Journal of Atmospheric and Oceanic Technology*, *27*, 3–22.

Goodman, S. J., Blakeslee, R. J., Koshak, W. J., Mach, D., Bailey, J., Buechler, D., et al. (2013). The GOES-R Geostationary Lightning Mapper. *Atmospheric Research*, *125-126*, 34–49.

Hilburn, K., Fuchs, B., & Rutledge, S.A. (2019). Evaluation of GOES-16 GLM to lightning mapping arrays, Paper presented at Ninth Conference on Meteorological Applications of Lightning Data, American Meteorological Society, Phoenix, AZ, recorded presentation at https://ams.confex.com/ams/2019Annual/videogateway.cgi/id/50561?recordingid=50561

Holle, R. L. (2014). Diurnal variations of NLDN-reported cloud-to-ground lightning in the United States. *Monthly Weather Review*, *142*, 1037–1052. https://doi.org/10.1175/MWR-D-13-00121.1

Murphy, M. J. (2006). *When flash algorithms go bad*. Paper presented at First International Lightning Meteorology Conference. Tucson, AZ: Vaisala, Inc.

Murphy, M. J. (2017). Preliminary results from the inclusion of lightning type and polarity in the identification of severe storms, Paper presented at Eighth Conference on Meteorological Applications of Lightning Data, American Meteorological Society, Seattle, WA.

Murphy, M. J. (2019). The next evolution of central processor in the U.S. National Lightning Detection Network, Paper presented at Ninth Conference on Meteorological Applications of Lightning Data, American Meteorological Society, Phoenix, AZ, recorded presentation at https://ams.confex.com/ams/2019Annual/videogateway.cgi/id/50728?recordingid=50682

Murphy, M. J., & Nag, A. (2015). Cloud lightning performance and climatology of the U.S. based on the upgraded U.S. National Lightning Detection Network, Paper presented at Seventh Conference on Meteorological Applications of Lightning Data, American Meteorological Society, Phoenix, AZ.

Murphy, M. J., & Said, R. K. (2018). Toward lightning mapping with long-baseline LF networks, Paper presented at 25th International Lightning Detection Conference and 7th International Lightning Meteorology Conference, Vaisala Inc., Ft. Lauderdale, FL.

NCEI (National Centers for Environmental Information) (2018). *Storm Data*, *60*(7).

Orville, R. E., Huffines, G. R., Burrows, W. R., & Cummins, K. L. (2011). The North American Lightning Detection Network (NALDN)—Analysis of flash data: 2001–09. *Monthly Weather Review*, *139*, 1305-1322. https://doi.org/10.1175/2010MWR3452.1

Rudlosky, S. D., Peterson, M. J., & Kahn, D. T. (2017). GLD360 performance relative to TRMM LIS. *Journal of Atmospheric and Oceanic Technology*, *34*, 1307–1322.

Schmit, T. J., Griffith, P., Gunshor, M. M., Daniels, J. M., Goodman, S. J., & Lebair, W. J. (2017). A closer look at the ABI on the GOES-R series. *Bulletin of the American Meteorological Society*, *98*, 681–698.

Schultz, C. J., Carey, L. D., Schultz, E. V., & Blakeslee, R. J. (2015). Insight into the kinematic and microphysical processes that control lightning jumps. *Weather and Forecasting*, *30*, 1591–1621.

Schultz, C. J., Carey, L. D., Schultz, E. V., & Blakeslee, R. J. (2017). Kinematic and microphysical significance of lightning jumps versus non-jump increases in total flash rate. *Weather and Forecasting*, *32*(1), 275–288. https://doi.org/10.1175/WAF-D-15-0175.1

Schultz, C. J., Petersen, W. A., & Carey, L. D. (2009). Preliminary development and evaluation of lightning jump algorithms for the real-time detection of severe weather. *Journal of Applied Meteorology*, *48*, 2543–2563.

Schultz, C. J., Petersen, W. A., & Carey, L. D. (2011). Lightning and severe weather: A comparison between total and cloud-to-ground lightning trends. *Weather and Forecasting*, *26*, 744–755.

Stolz, D. C., Rutledge, S. A., & Pierce, J. R. (2015). Simultaneous influences of thermodynamics and aerosols and deep convection and lightning in the tropics. *Journal of Geophysical Research*, *120*. https://doi.org/10.1002/2014JD023033

21698996, 2020, 5, Downloaded from https://agupubs.onlinelibrary.wiley.com/doi/10.1029/2019JD031172 by Capes, Wiley Online Library on [01/10/2025]. See the Terms and Conditions (https://onlinelibrary.wiley.com/terms-and-conditions) on Wiley Online Library for rules of use; OA articles are governed by the applicable Creative Commons License

Thomas, R. J., Krehbiel, P. R., Rison, W., Hunyady, S. J., Winn, W. P., Hamlin, T., & Harlin, J. (2004). Accuracy of the lightning mapping array. *Journal of Geophysical Research*, *109*, D14207.

Thomas, R. J., Krehbiel, P. R., Rison, W., MacGorman, D. R., Bruning, E. C., & Stanley, M. A. (2019). Evaluation of the GOES-R Geostationary Lightning Mapper (GLM) using ground-based Lightning Mapping Array (LMA) observations, Paper presented at Ninth Conference on Meteorological Applications of Lightning Data, American Meteorological Society, Phoenix, AZ, recorded presentation at https://ams.confex.com/ams/2019Annual/videogateway.cgi/id/50561?recordingid=50728

Thompson, R. L., Edwards, R., Hart, J. A., Elmore, K. L., & Markowski, P. (2003). Close proximity soundings within supercell environments obtained from the Rapid Update Cycle. *Weather and Forecasting*, *18*, 1243–1261.

Thompson, R. L., Edwards, R., & Mead, C. M. (2004a). An update to the supercell composite and significant tornado parameters, Paper presented at 22nd Conference on Severe Local Storms, American Meteorological Society, Hyannis, MA.

Thompson, R. L., Edwards, R., & Mead, C. M. (2004b). Effective storm-relative helicity in supercell thunderstorm environments, Paper presented at 22nd Conference on Severe Local Storms, American Meteorological Society, Hyannis, MA.

Thompson, R. L., Mead, C. M., & Edwards, R. (2004). Effective bulk shear in supercell thunderstorm environments, Paper presented at 22nd Conference on Severe Local Storms, American Meteorological Society, Hyannis, MA.

Thompson, R. L., Smith, B. T., Grams, J. S., Dean, A. R., & Broyles, C. (2012). Convective modes of significant severe thunderstorms in the contiguous United States. Part II: Supercell and QLCS tornado environments. *Weather and Forecasting*, *27*, 1136–1154.

Williams, E., Boldi, B., Matlin, A., Weber, M., Hodanish, S., Sharp, D., et al. (1999). The behavior of total lightning activity in severe Florida thunderstorms. *Atmospheric Research*, *51*, 245–265.

Yang, J., Zhang, Z., Wei, C., Lu, F., & Guo, Q. (2017). Introducing the new generation of Chinese Geostationary weather satellites, Fengyun-4. *Bulletin of the American Meteorological Society*, *98*, 1637–1658.

Zhang, D., & Cummins, K. L. (2019). Ground- and space-based observations of horizontally extensive lightning flashes, Paper presented at Ninth Conference on Meteorological Applications of Lightning Data, American Meteorological Society, Phoenix, AZ.

Zhu, Y., Rakov, V. A., Tran, M. D., & Nag, A. (2016). A study of National Lightning Detection Network responses to natural lightning based on ground truth data acquired at LOG with emphasis on cloud discharge activity. *Journal of Geophysical Research*, *121*, 14,651–14,660. https://doi.org/10.1002/2016JD025574

21698996, 2020, 5, Downloaded from https://agupubs.onlinelibrary.wiley.com/doi/10.1029/2019JD031172 by Capes, Wiley Online Library on [01/10/2025]. See the Terms and Conditions (https://onlinelibrary.wiley.com/terms-and-conditions) on Wiley Online Library for rules of use; OA articles are governed by the applicable Creative Commons License